Arch-trapped propagation in enclosed and free space biological objects

Per Olov Risman
School of Innovation, Design and Engineering
Mälardalen University
Vasteras, Sweden
per.olov.risman@mdh.se

Nikola Petrovic
School of Innovation, Design and Engineering
Mälardalen University
Vasteras, Sweden
nikola.petrovic@mdh.se

***Abstract*—The tendency of arch-trapped microwave propagation at curved surfaces is a kind of diffraction which needs more attention in the development of measurement systems, from the oil industry to the investigations using antenna applicator systems for biological objects. We develop equations for propagation in very lossy substances in metal pipes. Similar such propagation occurs at the periphery of rounded objects in air, where also surface wave effects occur and can cause measurement problems. We show a modified contacting antenna applicator minimizing arch-trapped as well as surface waves.**

Keywords—surface waves, microwave fields, microwave propagation, contacting antenna, contacting applicator.

I. INTRODUCTION

The probably most well-known example of arch-trapping is that of higher-order modes in circularly cylindrical metal pipes; see Fig. 1 [1]. An example of practical use of such TE_{mnp} modes of very high (m=18) order for heating of very large loads is given in [2].

We have since several years observed a number of issues relating to arch-trapped propagation and modes in lossy media, both in metal pipes and in and around objects under study (OUS) such as heads and breasts. Also the influences by contacting antenna/applicator designs are very important, in particular when attempting to avoid or reduce bolus volumes (then either as small contacting layers between antenna applicators and the OUS, or as larger volumes surrounding it).

A first example is related to determine oil/water/gas relative volumes in oilwell extraction pipes. The water is typically at the pipe walls and can have a high salt content. It can also be hot, which results in a quite strong attenuation of microwaves in the frequency range 1 to 3 GHz. Measurements with simple monopole antennas at the pipe periphery then show results which cannot been explained by simple TEM our spherical wave propagation.

A second example is in our investigations of antenna applicator designs for detection of breast tumors and brain hemorrhages by microwaves [3-5].

Related wavetypes are confined LSM and LSE modes, bound between a metallic or magnetic wall, respectively [6], but these are not dealt with here.

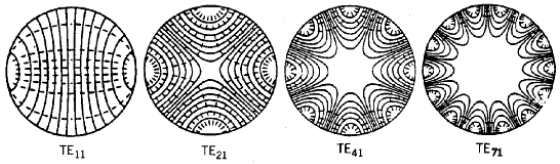

Fig. 1. Some circularly cylindrical TE modes.

II. ON TEM AND WAVEGUIDE MODE WAVELENGTHS IN A HOMOGENEOUS LOSSY MEDIUM

The plane wave unbound propagation equation for a lossy non-magnetic medium with complex permittivity $\varepsilon' - j\varepsilon''$ can be expressed as

$$E(z,t) = E(0)\cdot\exp\left[\,\mathrm{j}\omega t - \frac{2\pi}{\lambda_0}\cdot\mathrm{j}\left(\sqrt{\varepsilon' - j\varepsilon''}\right)z\right] \qquad (1)$$

It is seen that there will be a propagating wave with wavelength $\lambda_0 \big/ \mathrm{Re}\sqrt{\varepsilon' - \varepsilon''}$ accompanied by spatial losses $2\pi\cdot z \big/ (\lambda_0\ \mathrm{Im}\sqrt{\varepsilon' - \varepsilon''})$ in the direction of propagation.

The power penetration depth d_p becomes

$$d_p = \frac{-\lambda_0}{4\pi\ \mathrm{Im}\sqrt{\varepsilon}} \quad (plane\ wave) \qquad (2)$$

where λ_0 is the free space wavelength corresponding to the actual frequency. The d_p is the distance over which the power density is reduced by e (≈2,718). The field intensity has thus been reduced by a factor e over $2d_p$ and the attenuation over this skin depth distance d_s becomes 8,685 dB.

A mode is characterized by its critical frequency f_c and the quotient

$$f_c / f \equiv \nu \qquad (3)$$

is a very important parameter called the normalized wavelength[1]. Equation (1) is then modified into

[1] This also equivalent to $\sin\theta$, where θ is the (optical) incidence angle towards a dielectric boundary. Perpendicular incidence (θ=0°) thus corresponds to the plane wave case.

$$E(z,t) = E(0)\cdot\exp\left[\mathrm{j}\omega t - \frac{2\pi}{\lambda_0}\cdot\mathrm{j}\left(\sqrt{\varepsilon'(1-\nu^2)-j\varepsilon''}\right)z\right] \qquad (4)$$

Note that λ_0 is for a plane wave in empty space (i.e. ε =1) at the operating frequency. A first interesting consequence of (4) is that the equivalent wavelength in the dielectric is no longer $\lambda_0/\mathrm{Re}\sqrt{\varepsilon'-\varepsilon''}$ but instead $\lambda_0/\mathrm{Re}\sqrt{\varepsilon'(1-\nu^2)-\mathrm{j}\varepsilon''}$. This means that it becomes infinite for ν =1 (i.e. at f_c) only in the lossless dielectric case.

What happens with different ν values is very illustratively shown by use of the complex plane. Some features of lossy mode behavior are presented in such a graph (Fig. 2). – It is then to be noted that a complex number a –jb (having a polar angle $-\delta$ from the +Re axis, where δ = arctan($\varepsilon''/\varepsilon'$), and a length $\sqrt{a^2+b^2}$ has a square root with length $\sqrt[4]{a^2+b^2}$ and polar angle $-\delta/2$.

The first example in Fig. 2 (in red) is for a plane wave in a dielectric (i.e. no boundaries, TEM). The second example (blue in Fig. 2) is at ν =1 – i.e. at a mode f_c. Since there are losses, there is a resulting phase (only a mode in a lossless medium is in principle phaseless at ν =1). This corresponds to a smaller "effective mode ε' ", in the example about half the "standard" effective ε': blue ≈ $2{,}3^2$ ≈ 5,3 which is about the half of red $|\varepsilon|$= 10,4). The third example is with mode ν = 1,3 (green in Fig. 2). There is now a 180° phase change compared with ν < 1, i.e. a negative "effective mode ε' "

It is seen that the energy penetration depth decreases with increasing ν – as expected. Another conclusion of the above is that both attenuation and phase become complicated with modes in lossy media.

III. On Peripheral Wavelengths in a Very Lossy Medium Filling a Metal Pipe

It was shown in the preceding section that there will be a longitudinal propagation, albeit damped, at frequencies below the "cut-off" frequency as determined in the lossless case. The important consequence of this is that phase measurements are possible to carry out in transmitter/sensor "antenna" set-ups along metal pipes also in cases where the pipe is below "cut-off" with a lossless medium having the same real permittivity ε′ as the material under test in the pipe.

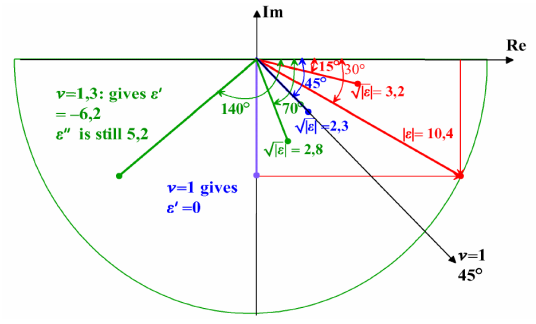

Fig. 2. Complex plane representation of lossy mode behavior with different ν values.

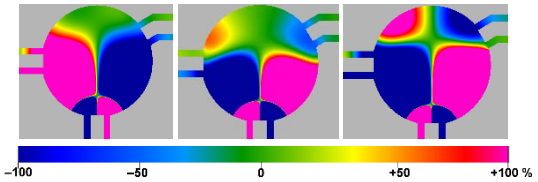

Fig. 3. Some circularly cylindrical TE modes. The scaling is "saturated" and related to momentaenous values.

There is, however, another intriguing propagation effect, now in the cross section plane of a circular pipe – and of course in the general case: along the curved surface. This arch-trapped TE-type propagation characteristics in a homogeneous lossy medium along the surface is different from the unbound propagation, due to the curvature.

A first observation is of the higher-order mode behaviour in an empty circular metal pipe. This is illustrated in the images in the Fig. 3, obtained by using the commercial software [7]. It is seen that the wavelength of the TE_{11} mode is 360°, and ¼ of that, i.e 90°, for the TE_{41} mode. Using the conventional formula for calculating the "cut-off" wavelength $\lambda_c = 2\pi a/x'_{n1}$ where a is the radius and x'_{n1} is the n:th zero of the cylindrical Bessel function derivative $J'_n(\rho)$ one obtains x'_{11}=1,841 and by that an 1,841 times shorter peripheral "cut-off" wavelength than that in free space (λ_0). For the TE_{41} mode the corresponding $x'_{41}/4$ is 1,329 which indicates that it approaches 1 for large n.

By using the function

$$c(n) = x'_{n1}/n \qquad (5)$$

and making a graph of tabulated Bessel function zeros as function of several integers n, the curve fit function becomes

$$c(n) \approx e^{0{,}655/\sqrt{n}-0{,}0434} \qquad (6)$$

It is obvious that n has to be an integer in the lossless case. However, if the losses are so large that that a full circular mode pattern will not be created, i.e. if the waves propagating in the opposite directions along the curved surface will be so damped by absorption that they do not interfere, n does no longer need to be an integer. This condition can actually also be represented by n for arbitrarily "sliced" wedge waveguides, for which non-integer n values can be calculated by analytical functions.

This "pure" arch-trapped mode type must obviously be considered to have particular properties due to the circumferential phase and attenuation behavior, by being guided by a concave metal surface creating a diffraction phenomenon in accordance with the Huygen's principle.

The simplest and most practical way to analyze what happens is by using numerical modelling. This was carried out with a diameter 102 mm metal pipe homogeneously filled with dielectric, and the modelled values at 250 and 400 MHz are shown in Table I, using the same software as before and throughout [7].

The resulting axial momentaneous H field is shown in the three images in Fig. 3. It is to be noted that the scaling was for saturation, allowing clear locations of the phase. – Left: ε'=1 and σ=2; mid: ε'=20 and σ=4; right: ε'=60 and σ=2. – It is clearly seen that the circumferential propagation is faster than the radial upwards.

TABLE I. NUMERICAL MODELLING DATA

Permittivities and wavelengths (λ = full wavelengths at pipe periphery)									
ε′	σ	ε″ @ 250M	ε″ @ 400M	*n*|*c*(*n*) @ 250M	*n*/*c*(*n*) @ 400M	Mod λ @ 250M	Calc λ @ 250M	Mod λ @ 400M	Calc λ @ 400M
1	2	144	90	1,61|1,60	—	≈226	225	—	—
1	5	360	225	2,54|1,44	—	122	129	—	—
20	2	144	90	1,71|1,58	2,26|1,48	204	209	144	148
20	4	288	180	2,34|1,47	—	136	147	—	—
20	5	360	225	2,61|1,44	3,34|1,37	116	125	102	93
60	2	144	90	1,97|1,53	2,76|1,42	170	164	112	116
60	5	360	225	2,76|1,42	3,64| 1,35	112	117	82	84

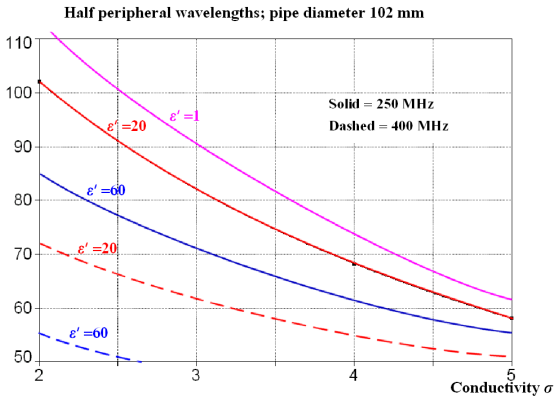

Fig. 4. Compilations of the runs in Table I.

The results from a number of runs with real permittivity ε′ from 2 to 60 and conductivity from 2 to 5 $\Omega^{-1}m^{-1}$ were carried out and the results are shown in the graph in Fig. 4.

The modelling results indicate the following approximate formula

$$\lambda_{arch} = \frac{\lambda_0}{\mathrm{Re}\sqrt{0,5 \cdot \varepsilon}} \tag{7}$$

where the factor $1/\sqrt{0,5} = \sqrt{2}$ is a canonical factor as usual in the geometric theory of diffraction. Comparisons with the results in the graph show that they are within about ±5 %, except for the $\varepsilon' = 1$; $\sigma = 2$ case. Now using the canonical constant $\sqrt{2}$, the first-order theoretical approximation of n becomes

$$n = \frac{2\pi a \cdot \mathrm{Re}\sqrt{\varepsilon}}{\lambda_0 \cdot \sqrt{2}} \tag{8}$$

where $\lambda_0 / (2\pi a \cdot Re\sqrt{\varepsilon})$ is the uncorrected number of wavelengths along 360° of the periphery, with a being the cylinder radius. The arch propagation wavelength then becomes

$$\lambda_{arch} = \frac{\lambda_0 \cdot c(n)}{\mathrm{Re}\sqrt{\varepsilon}} \tag{9}$$

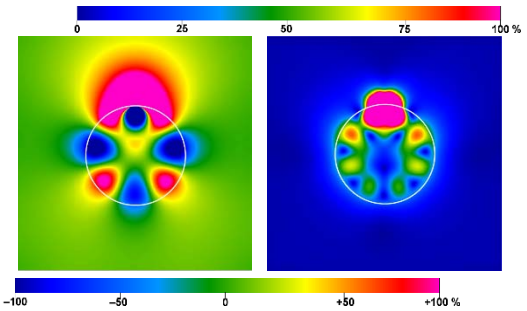

Fig. 5. Fields with 550 MHz (free space wavelength 545 mm) excitation of a 150 mm diameter long cylinder with ε′ = 50; ε″ = 3,27 (corresponding to σ = 0,1) was chosen for the mode studies. Field types: see text. The upper scale is for the right image (average value), and the scale at the bottom is related to the left image (momentaneous value).

The λ_{arch} values from (9) are also given in Table I, showing a quite acceptable agreement also for the $\varepsilon' = 1$; $\sigma = 2$ case. Equation (9) is thus applicable for the arch-trapped propagation in a homogeneously filled pipe, provided the attenuation is so large that no circumferential standing wave pattern is created.

IV. On Arch-Trapped Propagation at a Lossy High-Permittivity Circularly Cylindrical Medium

It is obvious that the internal propagation in a high permittivity medium will be with an imperfect magnetic wall at the boundary to free space. In addition and in contrast to the case with a metal pipe, the imperfect boundary results in the internal mode pattern being quite influenced by the excitation. Typically, however, the same arch-trapped pattern results and is (axial) TE or TM, depending on the excitation. Fig. 5 shows the modeled result of an excitation by an x-directed (left-right) H_x field point source 3 mm inside the relatively low-loss circularly cylindrical object, in the 12 o'clock position. The left image shows the momentaneous z-directed E_z field, and the right shows the averaged "horizontal" H field ($H_x + H_y$). – It is seen that this is a TM_{31} type mode, and that the surface-parallel E_z field is leaking significantly, due to the limited ε' and the resonant condition. – The TM_{31} mode in a metal pipe has a critical frequency determined by

$$\frac{2\pi\sqrt{\varepsilon'}}{\lambda_0} = \frac{x_{31}}{a} \tag{10}$$

where a is the ("unknown") cylinder radius and the function is now $J_n(\rho)$. With $\lambda_0 = 545$ mm and $x_{31} = 6,380$ one obtains $2a \approx 157$ mm. This indicates that the equivalent "leaky diameter" is 4,4 % larger than the geometrical, which is 150 mm. The circumferential wavelength is thus only slightly larger than that in a metal pipe. The *c(n)* function dealt with above will be somewhat modified and also depends on the extent of total reflection of the internal fields at the boundary.

V. Breast Scenario with Two Different Contacting Antennas

A scenario consisting of a hemispherical breast was used. The diameter was 126 mm, with a downwards circularly cylindrical 26 mm high continuation, located on a 90 mm high

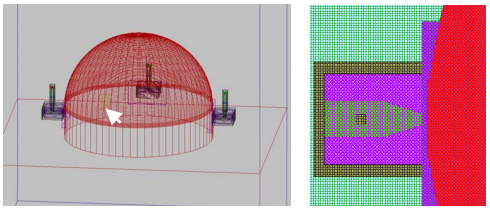

Fig. 6. The image to the right shows the scenario details of the "projectile" antenna and a "ceramic shape plate" contacting the breast. – The interior antenna materials are ZrO_2 ($\varepsilon' = 35$, greenish), surrounded by a cast material ($\varepsilon' = 19$, $\sigma = 0{,}02$; see [8]). The shape plate (dark blue) has thickness 1,0…3 mm, cross section dimensions 30×20 mm and $\varepsilon' = 72$.

large block with breast data was used. I addition a "tumor" (see arrow and yellow color in the left Fig. 6) with dimensions 10×10×6 mm, located about 30 mm from the breast surface was introduced. The whole scenario was in free space with the following dielectric data breast: $\varepsilon' = 33$; $\sigma = 0{,}9$ and tumor: $\varepsilon' = 45$; $\sigma = 0{,}8$. The frequency was 1300 MHz.

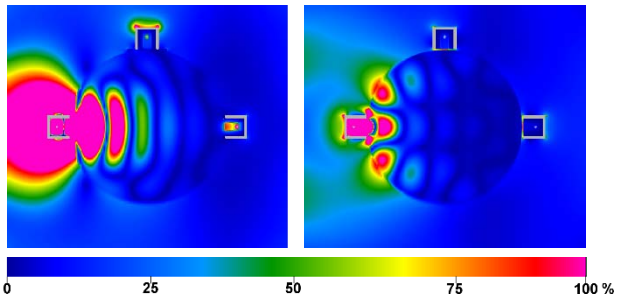

Fig. 7. The left image shows the momentaneous total E field in the "horizontal" z plane of the antennas in linear scaling, with the shape plate. The right image is the same but without the shape plate.

Two antenna cases were run; one with the shape plate as in the right Fig. 6, the other one without and the antenna being at 0.8 mm distance from the breast.

It is seen in the left images in Fig. 7 and Fig. 8 that there are neither surface nor arch-trapped waves excited.

The antenna excitation power in Fig. 7 was the same, and the equality applies also to Fig. 8. It is seen in both figures that the transmission efficiency is higher in the case with the shape plate.

It is concluded that the geometry and dielectric properties of the contacting part of antennas to object under study (OUS) is very important, and that simple impedance matching concepts need not be valid.

VI. Conclusion

It seems as these phenomena (arch-trapping in particular, but also surface waves) which both reduce the reception of signals which have travelled through the OUS, have hitherto not been sufficiently dealt with in the area of medical tomography. By using large but impractical bolus tanks both surface waves and arch-trapped waves can be eliminated only if the real permittivity of the OUS and bolus liquid are equal.

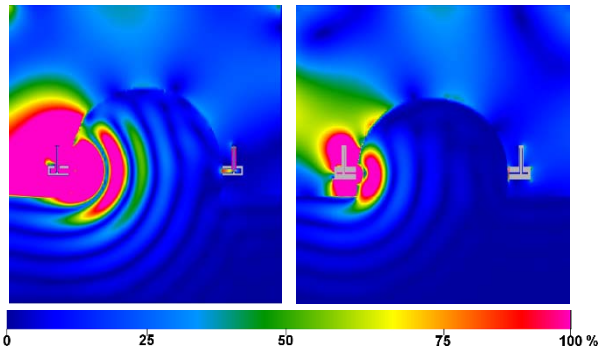

Fig. 8. The left and right image show the fields as in Fig. 7 but now in the vertical plane of the scenario. The amplitude scaling is equal in all images in Fig. 7 and 8.

Reduced bolus volumes and more advanced antenna applicators providing reduced excitation of these unwanted propagations will be necessary unless to-day's developments are to remain scientific excursions rather than practically useful systems that will be acceptable to the market.

References

[1] C.S. Lee et al "Plots of modal field distribution in rectangular and circular waveguides", IEEE Trans. MTT 1966.

[2] P.O. Risman et al, "Microwave system for heating voluminous elongated loads", Patent WO03053105A1, 2003.

[3] N. Petrovic, M. Otterskog and P. O. Risman, "Experiments and numerical modelling of contacting antenna applicators at a free space head model", 2015 IEEE Conference on Antenna Measurements & Applications (CAMA), Chiang Mai, 2015.

[4] N. Petrovic, M. Otterskog and P. O. Risman, "Antenna applicator concepts using diffraction phenomena for direct visualization of brain hemorrhages", 2016 IEEE Conference on Antenna Measurements & Applications (CAMA), Syracuse, NY, 2016,

[5] N. Petrovic, M. Otterskog and P. O. Risman, "Breast tumour detection by two microwave antenna principles", 2017 International Conference on Electromagnetics in Advanced Applications (ICEAA), pp. 1258-1261, Verona, 2017.

[6] Risman, P.O. "Confined modes between a lossy slab load and a metal plane as determined by a waveguide trough model", J Microwave Power and Electromagnetic Energy (JMPEE) 1987, Vol 22 No. 4, p 193-198.

[7] Quickwave™ 3D FDTD software package, *www.qwed.eu,* 2017.

[8] M. Otterskog, N. Petrovic and P. O. Risman, "A multi-layered head phantom for microwave investigations of brain hemorrhages", 2016 IEEE Conference on Antenna Measurements & Applications (CAMA), Syracuse, NY, 2016.